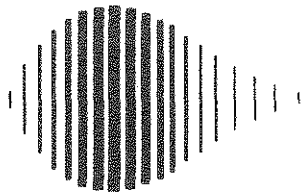

NATIONAL CENTER FOR EARTHQUAKE
ENGINEERING RESEARCH
State University of New York at Buffalo

SEISMIC PERFORMANCE ASSESSMENT OF CODE-DESIGNED STRUCTURES

by

Howard H.M. Hwang, Jing-Wen Jaw and How-Jei Shau
Center for Earthquake Research and Information
Memphis State University
Memphis, TN 38152

Technical Report NCEER-88-0007

March 20, 1988

This research was conducted at Memphis State University and was partially supported by the National Science Foundation under Grant No. ECE 86-07591.

NOTICE

This report was prepared by Memphis State University as a result of research sponsored by the National Center for Earthquake Engineering Research (NCEER). Neither NCEER, associates of NCEER, its sponsors, Memphis State University, nor any person acting on their behalf:

a. makes any warranty, express or implied, with respect to the use of any information, apparatus, method, or process disclosed in this report or that such use may not infringe upon privately owned rights; or

b. assumes any liabilities of whatsoever kind with respect to the use of, or for damages resulting from the use of, any information, apparatus, method or process disclosed in this report.

SEISMIC PERFORMANCE ASSESSMENT OF CODE-DESIGNED STRUCTURES

by

Howard H.M. Hwang[1], Jing-Wen Jaw[2] and How-Jei Shau[3]

March 20, 1988

Technical Report NCEER-88-0007

NCEER Contract Number 87-1004

NSF Master Contract Number ECE 86-07591

1 Associate Research Professor, Center for Earthquake Research and Information, Memphis State University
2 Post-Doctoral Research Associate, Center for Earthquake Research and Information, Memphis State University
3 Graduate Research Assistant, Center for Earthquake Research and Information, Memphis State University

NATIONAL CENTER FOR EARTHQUAKE ENGINEERING RESEARCH
State University of New York at Buffalo
Red Jacket Quadrangle, Buffalo, NY 14261

ABSTRACT

This report presents a method to assess the actual seismic performance of code-designed structures, in particular, shear wall structures. A probabilistic approach is used so that uncertainties in earthquake ground motions, structural responses, and structural capacities can be taken into consideration. Uncertainty in earthquake ground accelerations is explicitly accounted for by generating an ensemble of acceleration time histories from appropriate power spectral density functions and duration of strong motion. The modified Takeda hysteretic model is utilized to describe the nonlinear behavior of structures. The nonlinear seismic analyses are preformed to obtain the structural responses, which are then statistically analyzed. The statistics of the structural capacities can also be established based on the defined limit states. The performance of structures is measured in terms of the limit state probability, i.e., the probability that the structural response exceeds the structural capacity. The proposed method may be applied to various types of structures to evaluate the limit state probabilities. Given the limit state probabilities, the authority can consider the societal risk due to the occurrence of earthquakes and make decision on the appropriate level of earthquake protection.

TABLE OF CONTENTS

LIST OF ILLUSTRATIONS

LIST OF TABLES

SECTION 1
INTRODUCTION

The seismic performance of building structures is one of the main concerns in the design of structures. Conventional structures, in particular, low-rise buildings are usually designed according to provisions specified in building codes and standards such as Uniform Building Code (UBC) [1], Standard Building Code (SBC) [2] and American National Standard ANSI A58.1 [3]. The code provisions are intended to achieve satisfactory performance of buildings under various loads imposed by users or nature such as earthquakes during the lifetime of buildings in service. The satisfactory performance of buildings under earthquake loads means that buildings, designed according to the code provisions, will (1) resist minor earthquakes without any damage; (2) resist moderate earthquakes without significant structural damage, and (3) resist severe earthquakes without collapse. The above statement on seismic performance is described in a qualitative manner and the codes do not provide quantitative measure of the actual performance of the code-designed buildings.

Building codes usually employ simplified formulas in the provisions in order to facilitate the design process. For example, the equivalent static design forces are stipulated in building codes to represent the seismic forces which are dynamic and random in nature. Similarly, nominal structural capacity (resistance) is also specified by simplified formulas. The single design values determined by simplified formulas in building codes are for the design purpose. In reality, the actual structural capacity and loads imposed on structures are random in nature and involve other uncertainties. For example, we not only cannot predict the occurrence of an earthquake in advance, but also cannot precisely estimate its intensity and duration. In addition, structural responses are evaluated with idealized structural models. Thus, the structural responses computed under such conditions may exhibit considerable deviations from the actual structural responses. Furthermore, the structural capacity cannot be accurately determined since the basic parameters such as material strength always exhibit statistical variation. In view of uncertainties in loads, structural responses and structural capacities, it is of importance to evaluate the adequacy of these simplified formulas and their impact on the actual performance of code-designed buildings under earthquakes.

The objective of this study is to establish a general method to quantitatively assess the actual seismic performance of buildings which are designed according to the provisions of a

building code. The probabilistic approach is used so that the randomness and uncertainty in loads, structural responses and structural capacities can be taken into consideration. The performance of structures is measured in terms of the limit state probability, i.e., the probability that the structural response due to earthquakes exceeds the structural capacity which is established based on a defined failure criterion or limit state. This probability is called the limit state probability. Section 2 describes a general methodology for evaluating actual performance of code-designed structures under earthquakes, while Section 3 gives an example to illustrate the methodology. Then, Section 4 presents the summary and conclusions

SECTION 2
METHODOLOGY FOR ASSESSING SEISMIC PERFORMANCE

2.1 Design of Buildings

Most of the conventional buildings are designed according to provisions specified in a building code which is issued by a local authority. The local building code usually refers to a model building code with or without modifications. At present, there are four major model building codes in the United States: The BOCA/Basic Building Code [4], The National Building Code [5], The Standard Building Code [2], and Uniform Building Code [1]. All of these documents stipulate design requirements based on collective judgement of code committees.

In addition to these model codes, American National Standard ANSI A58.1 [3] considers only requirements for loads, not for structural capacity. Currently, ANSI A58.1 is being updated by a code committee organized by American Society of Civil Engineers (ASCE). Furthermore, ATC3-06 [6] is a proposed seismic design criterion developed by the Applied Technology Council. After an extensive trial design and modification process conducted by Building Seismic Safety Council (BSSC), ATC3-06 has become a recommended NEHRP seismic design provisions [7]. At present, the NEHRP provisions is being updated by BSSC for Federal Emergency Management Agency (FEMA). For designers and researchers as well, it is very difficult to understand the difference of these codes and to keep update with all the modifications. Thus, this leads to the debate on whether or not to have a model code for the entire United States [8].

In this study, the purpose of designing a structure is to evaluate the adequacy of the building code. Thus, a code-designed structure actually represents a class of structures located at sites where the building code has authority. For example, a 3-story shear wall building may represent many low-rise shear wall buildings designed under similar conditions.

2.2 Reliability Analysis of Buildings

Once a building has been designed according to an appropriate building code, a probabilistic approach is utilized to assess the actual structural performance under earthquakes so

that uncertainty in ground earthquake acceleration, structural response and structural capacity can be taken into consideration. Under severe earthquakes, the structural responses are usually in the nonlinear range. In order to realistically establish the statistical characteristics of nonlinear structural responses, the Monte Carlo simulation and nonlinear time history analysis are utilized in the reliability analysis. Figure 2-1 outlines a flow chart for the proposed reliability analysis method. The important features of the proposed method are described in the following sub-sections.

2.3 Nonlinear Seismic Analysis of Structures

A building is represented by a multi-degree-of-freedom (MDF) stick model fixed at the base as shown in Fig. 2-2. Each mass is assumed to have one degree of freedom, i.e., the horizontal displacement in the direction of earthquakes. The equations of motion for such an MDF system subjected to a horizontal earthquake ground acceleration is

$$[M]\{\ddot{X}\} + [C]\{\dot{X}\} + \{F_s\} = -[M]\{I\}\ a_g \tag{2.1}$$

where

$[M]$: mass matrix
$[C]$: damping matrix
$\{I\}$: identity vector
$\{X\}$: nodal displacement vector relative to the fixed base
$\{F_s\}$: restoring force vector
a_g: earthquake ground acceleration

The mass of the building is discretized at the mid-height of each story and lumped at the floor level. Thus, the mass matrix $[M]$ is a diagonal matrix. The damping matrix $[C]$ is taken as the Rayleigh damping matrix, which is the combination of the mass matrix $[M]$ and the initial stiffness matrix $[K_e]$ of the building system

$$[C] = a_0[M] + a_1[K_e] \tag{2.2}$$

where

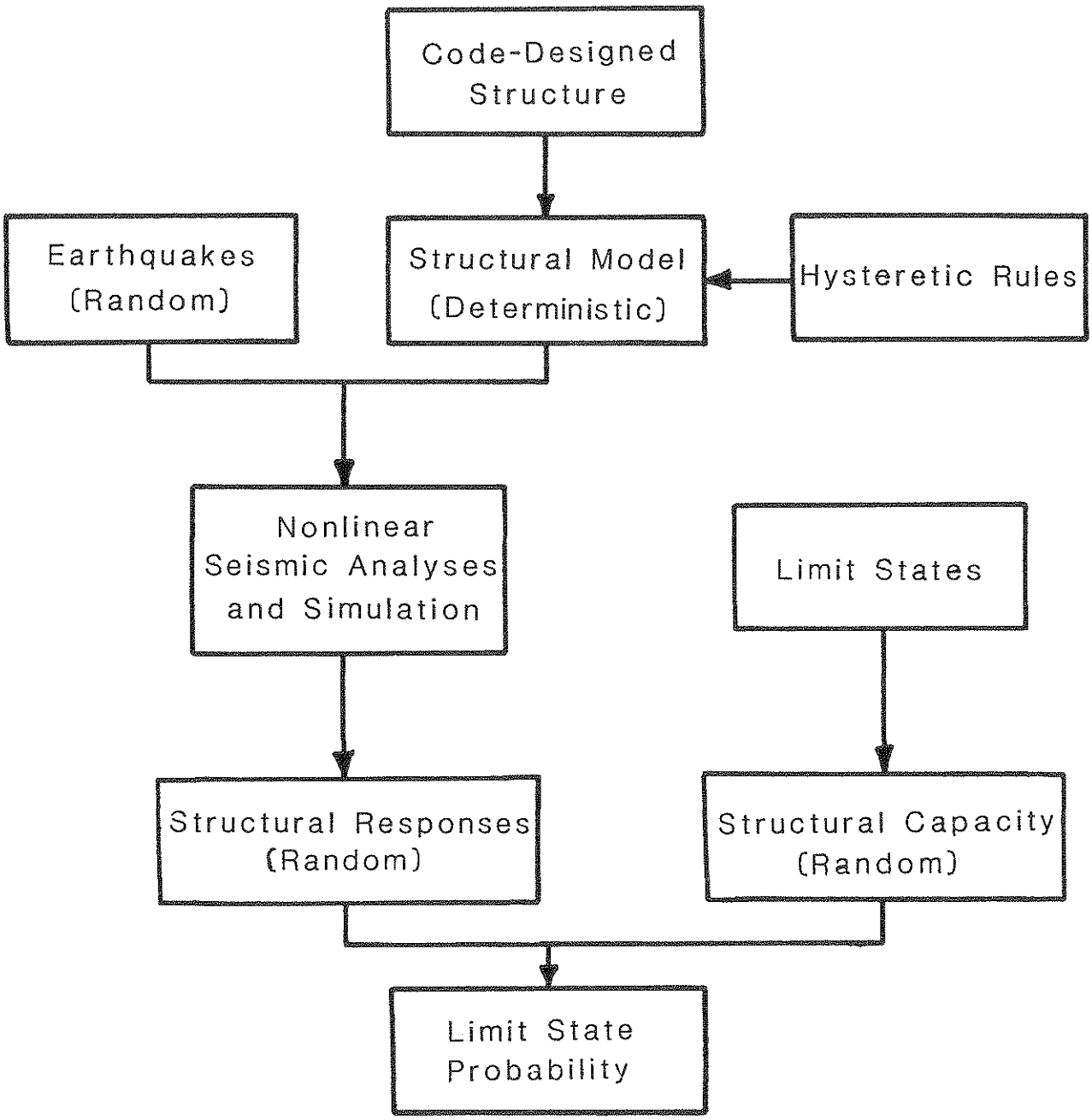

Fig. 2-1 Reliability Analysis Procedure

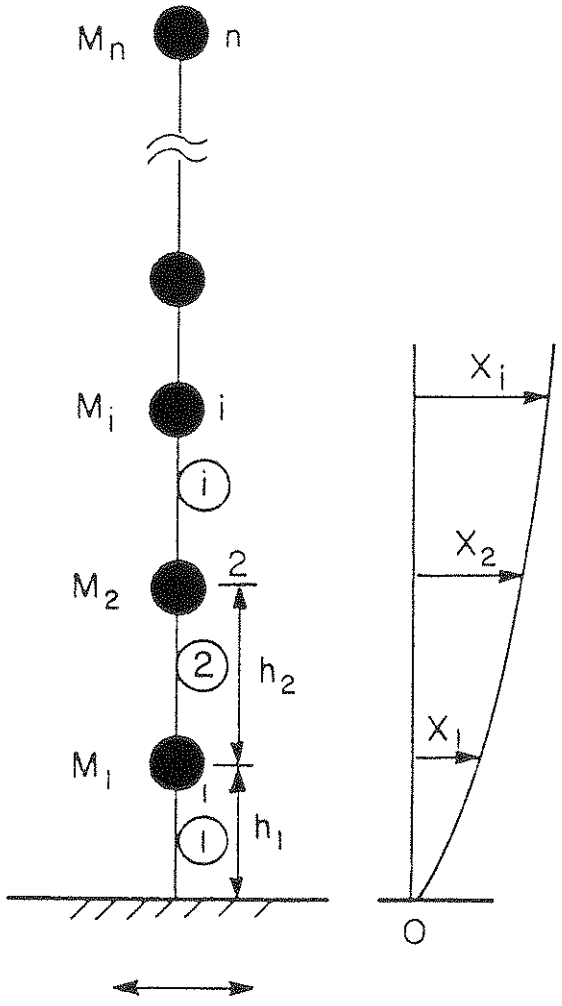

Fig. 2-2 Stick Model of Structure

$$a_0 = \frac{2\zeta\omega_1\omega_2}{\omega_1 + \omega_2}$$

and

$$a_1 = \frac{2\zeta}{\omega_1 + \omega_2} \tag{2.3}$$

in which ζ is the critical damping ratio; ω_1 and ω_2 are the first two natural circular frequencies of the structural system. From the free vibration analysis of the system, ω_1 and ω_2 are determined. The restoring force vector $\{F_s\}$ can be expressed in terms of the shear forces acting on the beam elements. The derivation of the restoring shear force is described in Section 2.4. In this study, the artificial earthquake time histories are utilized as seismic input and applied at the base of the structure. The generation of artificial earthquakes is discussed in Section 2.5. For a given earthquake time history, the Newmark's beta method with beta equal to 1/4 is utilized to integrate the equations of motion in the time domain to obtain structural responses.

2.4 Hysteretic Behavior

The restoring shear force acting on a beam element is related to the relative displacement between the two adjacent masses. This displacement is denoted as the inter-node displacement. The response of a structure to severe earthquake may be in the nonlinear range. Under this situation, it is generally recognized that the degradation of structural stiffness and the pinching phenomenon, which are caused by the opening and closing of the shear cracks during the cyclic loadings, present in the hysteretic curves. In this study, the modified Takeda model [9] as shown in Fig. 2-3 is used to describe the hysteretic characteristics of the restoring shear force and inter-node displacement. This modified Takeda model has a bilinear skeleton curve and includes both stiffness degrading and pinching effects.

2.4.1 Skeleton Curve

The hysteretic curve resulting from static monotonic increasing loading is called the skeleton curve. The shear force-displacement relationship under cyclic loads is usually enveloped by this curve. In this study, a bilinear skeleton curve shown in Fig. 2-4 is adopted for each beam element. In Fig. 2-4, (U_y, Q_y) is the idealized yielding point at which rebars

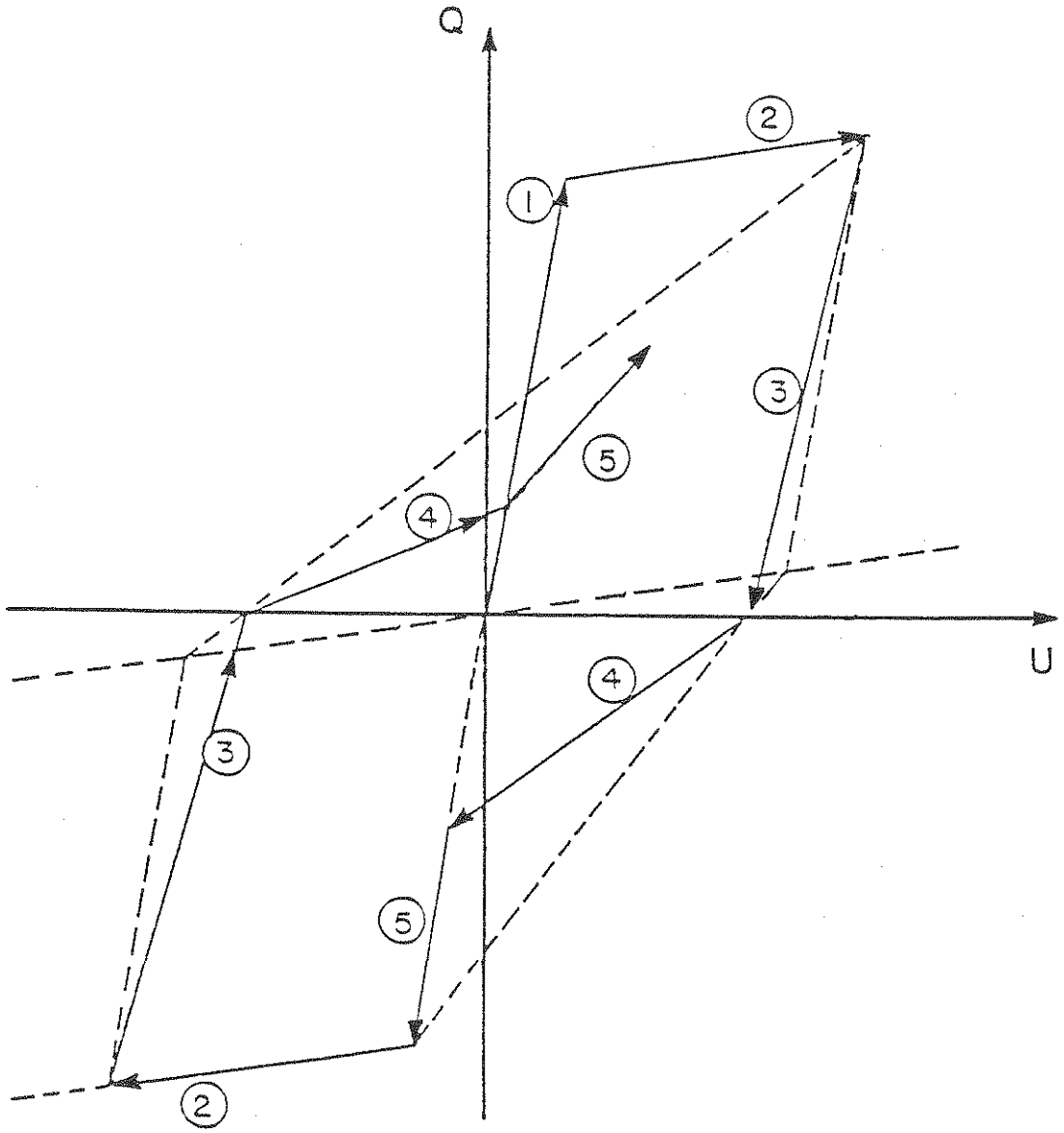

Fig. 2-3 Hysteretic Diagram

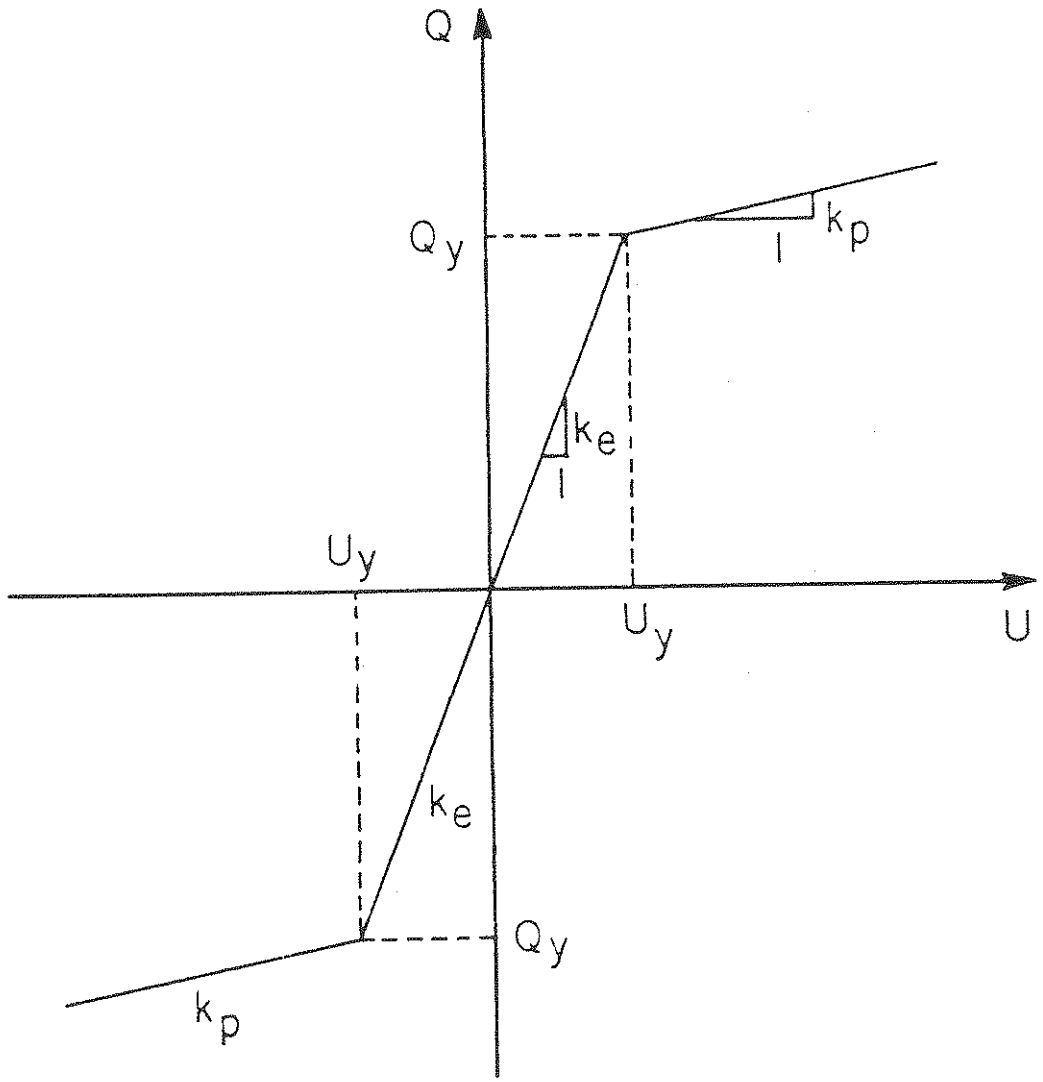

Fig. 2-4 Skeleton Curve

begin to yield. Furthermore, k_e and k_p represent the initial and post-yielding stiffness, respectively. The initial stiffness k_e is

$$k_e = Q_y/U_y \tag{2.4}$$

and the post-yielding stiffness k_p is expressed as

$$k_p = \alpha_s k_e \tag{2.5}$$

where α_s is the post-yielding slope factor.

2.4.2 Hysteretic Rules

The modified Takeda model is essentially governed by the following five rules:

1. Elastic loading and unloading with initial stiffness.
2. Inelastic loading with post-yielding stiffness.
3. Inelastic unloading with degrading stiffness.
4. Inelastic pinched reloading.
5. Peak oriented inelastic reloading.

These five rules result in five possible paths in the hysteretic diagram as identified in Fig. 2-3 by corresponding numbers in circles.

1) Elastic loading and unloading with initial stiffness

If the shear force (absolute value) never exceeds the yielding shear strength Q_y, then,

$$Q = k_1 U \tag{2.6}$$

where k_1 is equal to k_e.

2) Inelastic loading with post-yielding stiffness

If the shear force (absolute value) exceeds the yielding shear strength for the first time or exceeds the maximum inelastic shear force reached in any previous cycles, furthermore, if the shear force (absolute value) is still increasing, then,

$$Q = k_2 U + (Q_y - k_2 U_y) \tag{2.7}$$

where k_2 is equal to k_p.

3) Inelastic unloading with the degrading stiffness

If the yielding limit has been exceeded in previous cycles, and if the absolute value of the shear force is decreasing and the sign of shear force does not change, then,

$$Q = k_3 U + (Q_{mc} - k_3 U_{mc}) \tag{2.8}$$

where (U_{mc}, Q_{mc}) is the maximum point reached during the current loading cycle. The determination of k_3 is illustrated in Fig. 2-5.

$$k_3 = \frac{Q_{mc}}{U_{mc} - U_r} \tag{2.9}$$

The residual inter-nodal displacement at the zero shear force U_r can be determined as

$$U_r = U_0 - \frac{Q_0}{k_n} \tag{2.10}$$

and

$$k_n = \frac{Q_m - Q_0}{U_m - U_0} \tag{2.11}$$

where k_n is the stiffness of the reversed loading branch without considering pinching effect, and (U_m, Q_m) is the maximum point reached during any of the previous loading cycles in the reversed loading direction. (U_0, Q_0) is located at the intersection of two straight lines: one line passing through (U_{mc}, Q_{mc}) with the slope of k_e, and the other line passing through the origin with the slope of k_p. Hence, the coordinate (U_0, Q_0) can be expressed as

$$U_0 = \frac{1}{1 - \alpha_s}(U_{mc} - \frac{Q_{mc}}{k_e}) \tag{2.12}$$

$$Q_0 = \frac{\alpha_s}{1 - \alpha_s}(U_{mc} k_e - Q_{mc}) \tag{2.13}$$

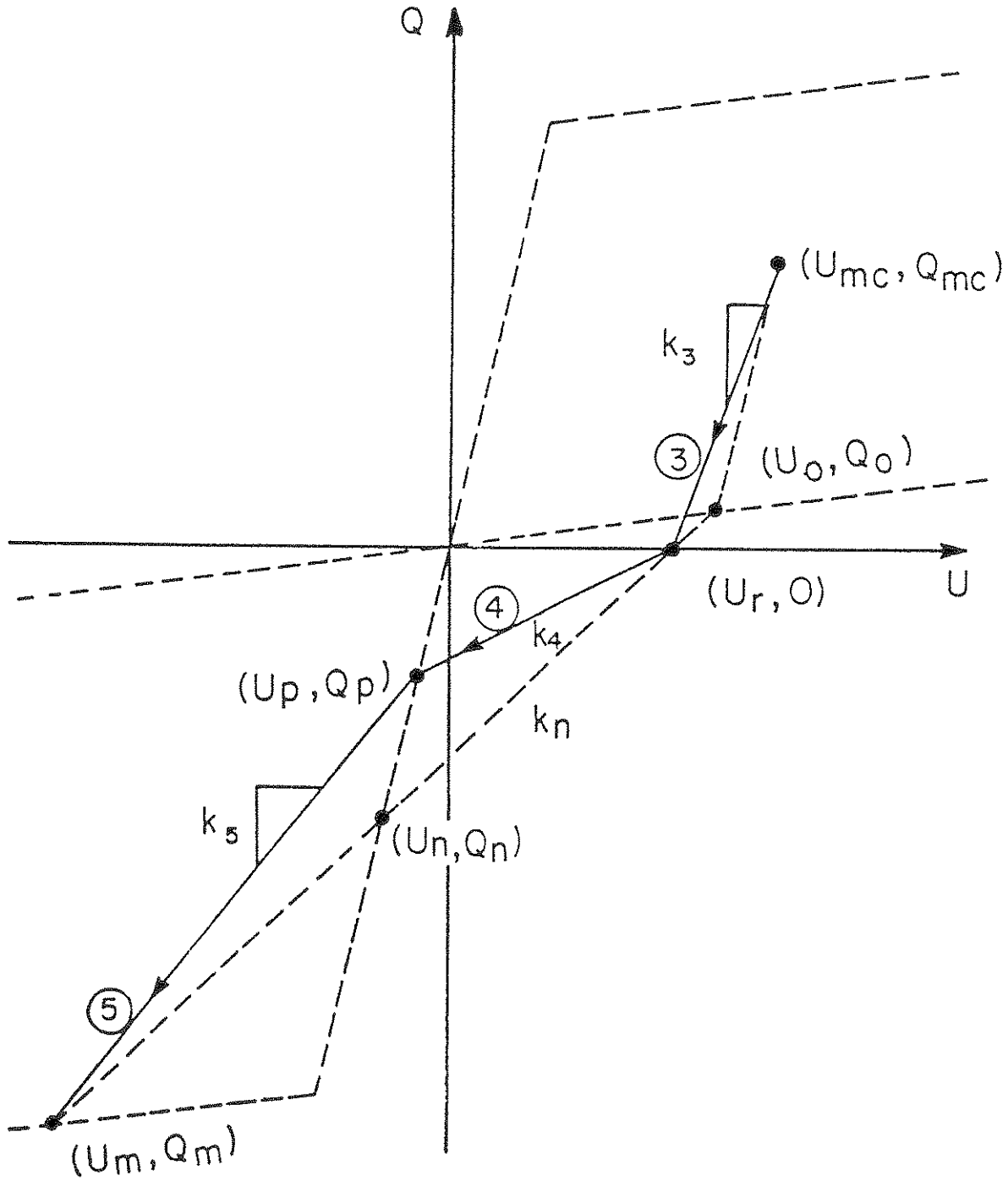

Fig. 2-5 Unloading and Reloading Stiffness

It is noted that k_3 is smaller than k_e if α_s is larger than zero. Thus, k_3 represents the degrading stiffness during the unloading cycles.

4) Inelastic pinched reloading

The opened shear cracks tend to close under reversed loading and it causes a significant increase in stiffness. This leads to a "pinched" shape of the hysteretic curve. In a reversed loading cycle, if the absolute value of the shear force is increasing but less than a pinching value, then

$$Q = k_4 U + (-k_4 U_r) \tag{2.14}$$

The stiffness k_4 can be expressed as

$$k_4 = \frac{-Q_p}{(U_r - U_p)} \tag{2.15}$$

where (U_p, Q_p) represents a pinching point and is defined as

$$U_p = \alpha_p U_n \tag{2.16}$$

$$Q_p = \alpha_p Q_n \tag{2.17}$$

in which α_p is a pinching factor and (U_n, Q_n) represents a point with no pinching effect.

$$U_n = U_r(\frac{k_n}{k_n - k_e}) \tag{2.18}$$

$$Q_n = k_e U_n \tag{2.19}$$

5) Peak oriented inelastic reloading

In a reversed loading cycle, if the shear force (absolute value) is increasing and exceeds the shear force at the pinching point defined by Eqs. 2.16 and 2.17, then

$$Q = k_5 U + (Q_p - k_5 U_p) \tag{2.20}$$

where

$$k_5 = \frac{Q_m - Q_p}{(U_m - U_p)} \tag{2.21}$$

As shown in Eqs. 2.6-2.8, 2.14 and 2.20, the restoring shear force Q can be expressed in terms of the inter-node displacement U. In general, these equations can be written as

$$Q = kU + s \tag{2.22}$$

where s is the expression in the parenthesis in those equations. For an MDF system, the restoring shear force for the i-th element Q_i can be written in the same way as Eq. 2.22.

$$Q_i = k_i U_i + s_i \tag{2.23}$$

where

$$U_i = X_i - X_{i-1} \tag{2.24}$$

in which X_i is the i-th nodal displacement relative to the fixed base. The restoring force vector $\{F_s\}$ is

$$\{F_s\} = \begin{pmatrix} Q_1 - Q_2 \\ Q_2 - Q_3 \\ \vdots \\ Q_n \end{pmatrix} \tag{2.25}$$

where Q_i is the restoring shear force acting on the beam element i. Substituting Eqs. 2.23 and 2.24 into Eq. 2.25, $\{F_s\}$ can be expressed as

$$\{F_s\} = [K]\{X\} + \{S\} \tag{2.26}$$

in which the tangential stiffness [K] is formed by the summation of the appropriate k_i, and the vector $\{S\}$ is

$$\{S\} = \begin{pmatrix} s_1 - s_2 \\ s_2 - s_3 \\ \vdots \\ s_n \end{pmatrix} \tag{2.27}$$

2.5 Artificial Earthquake Time Histories

Two basic approaches are generally utilized to represent ground motions. One approach is to use recorded ground accelerograms to represent earthquakes that may be expected at a site. Although the number of records has increased in past decades, there is a scarcity of strong motion records for some regions, for example, the eastern U.S. Aside from the lack of records, this approach does not grasp the variation of future earthquakes and reflect the local site conditions. These concerns give rise to the use of simulated artificial earthquake time histories to represent ground motions. Many methods for generating artificial earthquakes have been proposed [10-14]. In this study, the approach to generate artificial earthquake time histories is based on a specified power spectral density function (power spectrum) and duration of strong motion.

The stationary acceleration time history $a(t)$ is simulated by the following expression [12].

$$a(t) = \sqrt{2} \sum_{k=1}^{N_f} \sqrt{S_g(w_k)\Delta\omega} cos(\omega_k t + \phi_k) \tag{2.28}$$

where

$S_g(\omega)$: one-sided earthquake power spectrum
N_f: number of frequency intervals
$\Delta\omega$: ω_u / N_f
ω_u: cutoff frequency
ω_k: $k\Delta\omega$
ϕ_k: random phase angle uniformly distributed between 0 and 2π

The power spectrum used in this study is a Kanai-Tajimi power spectrum [15].

$$S_g(\omega) = S_0 \frac{1 + 4\zeta_g^2 \left(\frac{\omega}{\omega_g}\right)^2}{[1 - \left(\frac{\omega}{\omega_g}\right)^2]^2 + 4\zeta_g^2 \left(\frac{\omega}{\omega_g}\right)^2} \tag{2.29}$$

where S_0 is the intensity of the spectrum which is related to the peak ground acceleration [16]. Parameters ω_g and ζ_g are the dominant ground frequency and the critical damping, respectively, which depend on the site soil condition.

The normalized nonstationary time history $a_m(t)$ is obtained by applying an envelope function $f(t)$ to a stationary time history $a(t)$, and then divided by the maximum value of the time history a_{max}.

$$a_m(t) = \frac{a(t)f(t)}{a_{max}} \tag{2.30}$$

The artificial nonstationary time history $a_g(t)$ is the product of a specified peak ground acceleration PGA and a normalized nonstationary time history $a_m(t)$.

$$a_g(t) = PGA \times a_m(t) \tag{2.31}$$

The peak ground acceleration has been commonly used as the parameter to characterize ground motion in seismic hazard study. Seismic hazard at a site may be described in terms of the probability distribution of peak ground acceleration. This study suggests to check the actual performance of structures at two PGA levels. For the lower level, the PGA value with 10 percent exceedance probability in 50 years is selected and denoted as the maximum probable earthquake. For the higher level, the PGA value with 10 percent probability of being exceeded in 250 years is selected and denoted as the maximum credible earthquake.

2.6 Uncertainty Analysis

As described in Section 1, uncertainties exhibit in earthquake ground motion and structural system. An attempt to deal with all uncertainties using a Latin hypercube simulation technique is described in Ref. 17. In this study, uncertainties in structures are not included and best estimated values are used for structural properties. On the other hand, given a PGA level, uncertainties in earthquake ground acceleration is quantified by random phase angles and power spectral density functions. In this study, from each power spectrum, a set of acceleration time histories are generated using random phase angles.

2.7 Probabilistic Structural Responses

For each artificial earthquake, the nonlinear seismic analysis method described in Section 2.3 is utilized to evaluate the responses of the building, e.g., the story ductility ratios of all stories. The story ductility ratio of i-th story is defined as the ratio of the maximum absolute inter-story displacement $U_{max,i}$ to the yielding displacement $U_{y,i}$.

$$\mu_i = U_{max,i}/U_{y,i} \tag{2.32}$$

The maximum ductility ratio of the structure μ_E is the largest value chosen among all story ductility ratios

$$\mu_E = max(\mu_i) \tag{2.33}$$

The values of μ_E obtained under all artificial earthquakes exhibit variations. It has been suggested that the peak responses are fitted well by an extreme Type I distribution [18]. Thus, in this study, the maximum ductility ratio is assumed to be extreme Type I distributed. The cumulative distribution function of the extreme Type I variable S can be expressed as

$$F_S(s) = exp[-exp(-\alpha(s-u))] \tag{2.34}$$

where α and u are constants and determined by the following formulas [19].

$$u = \bar{S} - 0.5772/\alpha \tag{2.35}$$

$$\alpha = \pi/(\sqrt{6}\sigma_S)$$

where $\bar{S}$ and σ_S are the sample mean and the sample standard deviation of S, respectively.

2.8 Limit States and Structural Capacities

A limit state generally represents a state of undesirable structural behavior, for example, structural collapse or instability. For a structural system, it is likely that more than one limit state has to be considered. Damage of a structure due to earthquakes may be measured by a single large nonlinear excursion undergone by the structure (brittle structure) or by the amount of energy dissipated during inelastic cycling (ductile structure). The presence of nonlinear behavior makes it difficult to formulate limit states based on strengths of the structure. Seismic limit states of a structure should reflect nonlinear dynamic behavior and damage incurred in a structure.

Various damage models which incorporate maximum deformations and/or energy dissipation have been proposed [20]. However, the use of energy-related damage model to define limit states sometimes is difficult due to the lack of experimental data. Traditionally, the ductility ratio is used to characterize inelastic structural responses. It can be used to correlate the levels of structural damage and thereby define limit states. Two limit states representing moderate structural damage and collapse of the structure are considered in this study. For each limit state, a corresponding capacity in terms of maximum ductility ratio can be established. The structural capacity R is usually modeled by a lognormal distribution [21].

$$R = LN(\tilde{R}, \beta_R) \tag{2.36}$$

where LN stands for the lognormal variable; $\tilde{R}$ is the median value and β_R is the logarithmic standard deviation, i.e., the standard deviation of lnR, respectively. Usually, $\tilde{\mu}_R$ and β_R are determined by analyzing approximate data.

2.9 Limit State Probability

The limit state probability is used as a measure of structural performance in this study. The limit state probability P_f is defines as the probability of structural response S exceeds structural capacity R. It can be shown [19] that the limit state probability may be written as:

$$P_f = P_r(R \leq S) = \int_{r=0}^{\infty} (1 - F_S(r)) f_R(r) dr \tag{2.37}$$

where $F_S(\cdot)$ is the cumulative probability distribution of S and $f_R(\cdot)$ is the probability density function of R. In this study, S and R are assumed to be extreme Type I and lognormal distributed, respectively. Thus, no closed-form solution for P_f is available and it is necessary to perform numerical integration on Eq. 2.37 in order to evaluate limit state probability.

SECTION 3
ILLUSTRATIVE APPLICATION

A three-story office building assumed to be located in Memphis is chosen to demonstrate the general methodology described in Section 2. A typical floor plan and section is shown in Fig. 3-1. A steel frame system is used to resist gravity loads, i.e., dead and live loads. In order to resist seismic forces, four bays at corners of the building in the east-west direction are braced, while two reinforced concrete shear walls are used in the north-south direction as shown in Fig. 3-1. It is noted that, for such a structural system, the damage incurred in shear walls represents the similar damage of the entire building. Thus, this report is focused on the design and the assessment of these two shear walls.

3.1 Structural Loads

Three types of loads, i.e., dead, live and earthquake loads are considered to act on the building. The design values of dead and live loads are tabulated in Table 3-I. The tributary area for each shear wall is 30 ft. $\times$ 50 ft. Thus, the dead and live loads acting on each shear wall are calculated and shown in Table 3-II and 3-III, respectively.

The design seismic base shear V specified in ANSI A58.1-1982 is as follows:

$$V = ZIKCSW \tag{3.1}$$

where

- V: total shear force at the base
- Z: zone factor
- I: importance factor
- K: building system factor
- C: numerical coefficient
- S: soil factor
- W: total dead load of the building

According to the map for seismic zones in ANSI A58.1-1982, Memphis is located in seismic zone 3 and thus Z is equal to 3/4. The importance factor I and building system factor K are taken to be 1.0. The coefficient C is determined by

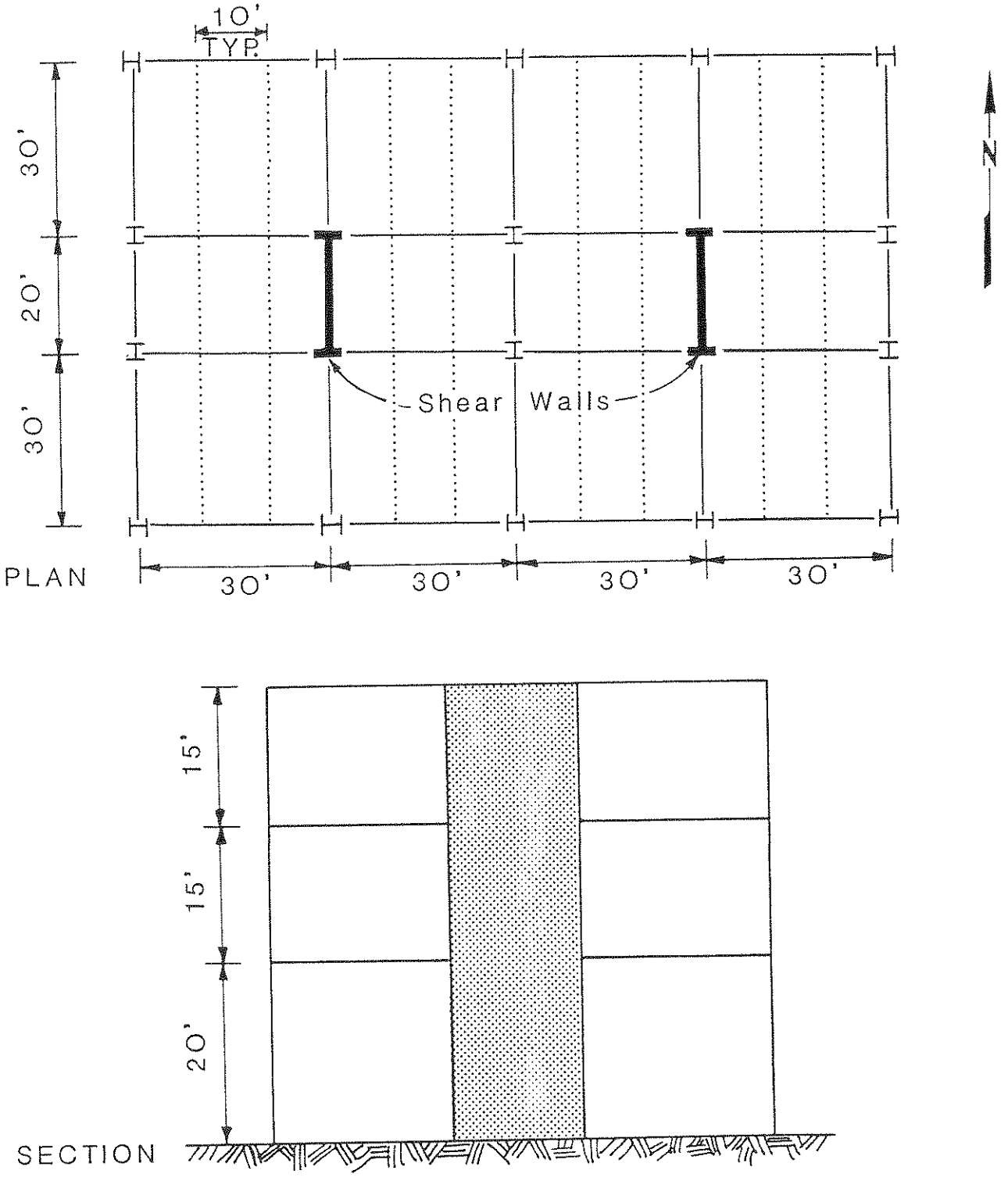

Fig. 3-1 Plan and Section of Office Building.

Table 3-I Unit Dead and Live Loads

Dead Load :		
Roof (4″ slab and insulation)	52	psf
Floor (5″ slab and ceiling)	67	psf
Girder ($W18 \times 86$)	86	plf
Beam ($W18 \times 60$)	60	plf
Column ($W14 \times 90$)	90	plf
Exterior Wall (curtain wall)	8	psf
Interior Partition (4″ gypsum block)	13	psf
Shear Wall (5″ reinforced concrete)	62.5	psf
Live Load :		
Roof*	25	psf
3rd and 2nd Floor	50	psf

*Live load for roof is assumed to be one-half of the value specified for office area.

Table 3-II Dead Load for Each Shear Wall

Roof:		Weight (lbs)
Roof Slab	$52 \times 30 \times 50$	78000
Girder	$86 \times 30 \times 2$	5160
Beam	$60 \times (50 \times 2 + 15 \times 2)$	7800
Subtotal		90960
2nd and 3rd Floor:		
Floor Slab	$67 \times 30 \times 50$	100500
Girder	$86 \times 30 \times 2$	5160
Beam	$60 \times (50 \times 2 + 15 \times 2)$	7800
Interior partition	$13 \times 30 \times 15$	5850
Shear wall	$((18 \times 12 \times 2) + (5 \times 216))$	
	$\times 150 \times 15 \times 1/144$	23625
Subtotal		285870
1st Floor:		
Shear wall	$((18 \times 12 \times 2) + (5 \times 216))$	
	$\times 150 \times 2 \times 10 \times 1/144$	31500
Total Dead Load		408330 = 408 kips

Table 3-III Live Load for Each Shear Wall

		Weight (lbs)
Roof	$25 \times 30 \times 50$	37500
2nd and 3rd Floor	$50 \times 30 \times 50$	75000
Total Live Load		187500 = 187.5 kips

$$C = \frac{1}{15\sqrt{T}} \tag{3.2}$$

in which T is the fundamental period of the building in seconds. For a building with shear walls, T can be computed by the following formula

$$T = \frac{0.05 h_n}{\sqrt{D}} \tag{3.3}$$

where h_n is the building height from the base and D is the dimension of the building in the direction parallel to the applied seismic forces. Referring to Fig. 3-1, h_n is 50 ft and D is 80 ft. Thus, T is determined as 0.28 sec. and C is equal to 0.126. The soil condition at the site of this office building is assumed to be classified as S_2. Thus, the soil factor S is 1.2. The product of numerical coefficient C and soil factor S is equal to 0.15. However, the ANSI A58.1-1982 specifies that the product CS need not exceed 0.14. Hence, CS is taken as 0.14 instead of 0.15. The total dead load of the building W is 2609 kips as shown in Table 3-IV. Thus, the seismic base shear V, determined from Eq. 3.1, is 273.95 kips. The base shear is distributed over the height of the structure.

$$F_x = \frac{(V - F_t) W_x h_x}{\sum_{i=1}^{n} W_i h_i} \tag{3.4}$$

where

F_x:	lateral force applied at level x
F_t:	additional concentrated lateral force at the top of structure
h_x, h_i:	height from the base to level x or i, respectively
W_x, W_i:	weight located or assigned to level x or i, respectively
n:	number of stories

According to ANSI A58.1-1982, F_t may be considered as zero when T is 0.7 sec. or less. In this case, T is 0.28 sec., thus, F_t is equal to zero. The calculation of F_x is shown in Table 3-V. From these lateral forces, the shear force and overturning moment at each floor level can be determined. The story shear and overturning moment at the base of the shear wall are 136.9 kips and 5168 ft-kips, respectively.

Table 3-IV Calculation of Total Dead Load

Roof:		Weight (lbs)
Roof	$52 \times 120 \times 80$	499200
Girder	$86 \times 120 \times 4$	41280
Beam	$60 \times (11 \times 80 + 4 \times 30)$	60000
Column	$90 \times 16 \times 7.5$	10800
Exterior wall	$8 \times (120 \times 2 + 80 \times 2) \times 7.5$	24000
Interior partition	$13 \times (120 + 80) \times 7.5$	19500
Shear wall	$((18 \times 12 \times 2) + (5 \times 216))$	
	$\times 150 \times 2 \times 7.5 \times 1/144$	23625
Subtotal		678405
3rd Floor:		
Floor	$67 \times 120 \times 80$	643200
Girder	$86 \times 120 \times 4$	41280
Beam	$60 \times (11 \times 80 + 4 \times 30)$	60000
Column	$90 \times 16 \times 15$	21600
Exterior wall	$8 \times (120 \times 2 + 80 \times 2) \times 15$	48000
Interior partition	$13 \times (120 + 80) \times 15$	39000
Shear wall	$((18 \times 12 \times 2) + (5 \times 216))$	
	$\times 150 \times 2 \times 15 \times 1/144$	47250
Subtotal		900330

Table 3-IV (Continued)

2nd Floor:		Weight (lbs)
Floor	$67 \times 120 \times 80$	643200
Girder	$86 \times 120 \times 4$	41280
Beam	$60 \times (11 \times 80 + 4 \times 30)$	60000
Column	$90 \times 16 \times 17.5$	25200
Exterior wall	$8 \times (120 \times 2 + 80 \times 2) \times 17.5$	56000
Interior partition	$13 \times (120 + 80) \times 17.5$	45500
Shear wall	$((18 \times 12 \times 2) + (5 \times 216))$	
	$\times 150 \times 2 \times 17.5 \times 1/144$	55125
Subtotal		926305
1st Floor:		
Column	$90 \times 16 \times 10$	14400
Exterior wall	$8 \times (120 \times 2 + 80 \times 2) \times 10$	32000
Interior partition	$13 \times (120 + 80) \times 10$	26000
Shear wall	$((18 \times 12 \times 2) + (5 \times 216))$	
	$\times 150 \times 2 \times 10 \times 1/144$	31500
Subtotal		103900
Total Dead Load		2608940 = 2609 kips

Table 3-V Distribution of Seismic Forces

Level	W_x(kips)	h_x(ft)	$W_x h_x$	F_x(kips)	$F_x/2$(kips)
Roof	678.4	50	33920	110.6	55.3
3rd Floor	900.3	35	31510.5	102.8	51.4
2nd Floor	926.3	20	18526	60.4	30.2
1st Floor	103.9	0	0	0	0
$\sum$	2609		83956.5	273.8	136.9

3.2 Combination of Loads

A structure should be designed to provide sufficient resisting capacity against the forces resulting from the combinations of loads acting on a structure. The load combinations specified in ANSI A58.1-1982 are

$$\phi R_n \geq \begin{cases} 1.4D \\ 1.2D + 1.6L \\ 1.2D + 0.5L + 1.5E \\ 0.9D - 1.5E \end{cases} \qquad (3.5a - 3.5d)$$

where

D: dead load effect
L: live load effect
E: load effect due to earthquake
ϕ: strength reduction factor
R_n: nominal capacity

It is assumed that the thickness of the wall is constant, thus, the cross section near the base of the shear wall is the critical section to be designed. On the basis of the individual loads described above, the factored axial force P_u, shear force V_u, and moment M_u at base of the shear wall due to various loading combinations are shown in Table 3-VI.

3.3 Design for Shear Force

The shear wall is designed according to ACI 318-83 [22]. Since there is no shear force resulting from gravity loads, Eqs. 3.5c and 3.5d can be rewritten as

$$\phi V_n \geq V_u \qquad (3.6)$$

where V_u is the design shear force at the base of the shear wall. As shown in Table 3-VI, V_u is equal to 205.4 kips. The nominal shear capacity V_n specified in ACI code is

$$V_n = V_c + V_s \qquad (3.7)$$

where V_c and V_s are the shear strength provided by concrete and shear reinforcement, respectively;

Table 3-VI Combinations of Load Effects

Case	Equation	P_u (kips)	V_u (kips)	M_u (ft-kips)
1	3.5a	571.6	0	0
2	3.5b	790.0	0	0
3	3.5c	583.7	205.4	7752
4	3.5d	367.5	205.4	7752

$$V_c = 2\sqrt{f'_c}\, td \tag{3.8}$$

$$V_s = A_v f_y d/s_2 \tag{3.9}$$

where A_v is the area of horizontal shear reinforcement within each vertical distance s_2; t is the thickness of shear wall; d is the distance from the extreme compressive fiber to center of tensile reinforcement and is equal to 0.8 ℓ_w, in which ℓ_w is the length of shear wall.

In this study, the compressive strength of concrete f'_c and the yield strength of reinforcement f_y are specified as 4000 psi and 60000 psi, respectively. Assuming the wall thickness is 5 in, the nominal shear strength provided by concrete is 121.4 kips (Eq. 3.8). As stated in ACI 318-83, the minimum horizontal reinforcement ratio ρ_h is 0.0025. For one layer of #3 rebars ($A_v = 0.11$ in^2), the maximum spacing $s_{2,max}$ to meet this minimum reinforcement ratio requirement is determined by

1. $s_{2,max} = A_v/t\rho_h = 8.8''$
2. $s_{2,max} = \ell_w/5 = 48''$
3. $s_{2,max} = 18''$
4. $s_{2,max} = 3t = 15''$

On the basis of these requirements, s_2 is set to be 8.5 in. and this produces a shear strength of 149 kips provided by shear reinforcement (Eq. 3.9). Therefore, the nominal shear capacity of the shear wall V_n is equal to 270.5 kips. The strength reduction factor ϕ for shear is 0.85 and thus ϕV_n is equal to 230 kips which is greater than the factored design shear force 205.4 kips.

With reference to ACI 318-83, the vertical shear reinforcement ratio ρ_n shall not be less than

$$\rho_n = 0.0025 + 0.5 \times (2.5 - h_w/\ell_w) \times (\rho_h - 0.0025) \tag{3.10}$$

where

ρ_h: horizontal shear reinforcement ratio

ℓ_w: horizontal length of wall

h_w: total height of wall from base to top (Note : h_w is the same as h_n)

From Eq. 3.10, ρ_n is determined as 0.0025. Also, the maximum spacing $s_{1,max}$ in the horizontal section of the shear wall must meet the same requirements as for $s_{2,max}$. Thus, one layer of #3 rebars with spacing of 8.5 in is used as vertical shear reinforcement.

3.4 Design for Axial Force and Moment

For members subjected to axial force with flexure, the strength reduction factor ϕ is 0.7 as specified in ACI code. The design for each case shown in Table 3-VI is described in the following.

1) Case 3 : $P_u = 583.7$ kips, $M_u = 7752$ ft-kips

In this case, the required nominal axial strength P_n and the nominal flexure strength M_n are given as

$$P_n = \frac{P_u}{\phi} = 834 \ \text{kips}$$

$$M_n = \frac{M_u}{\phi} = 11074.3 \ \text{ft} - \text{kips}$$

Thus, the eccentricity $e = M_n/P_n$ is 13.3 ft. The location of neutral axis is determined from the equilibrium of forces acting on the cross section of shear wall.

$$P_n = C_c + C_s - T \tag{3.11}$$

where

C_c: Compressive force due to concrete
C_s: Compressive force due to steel reinforcement
T: Tensile force due to steel reinforcement

It is assumed that both tensile and compressive reinforcements yield. Thus,

$$T = A_s f_y \tag{3.12}$$

$$C_s = A'_s f_y \tag{3.13}$$

in which A_s and A'_s are the area of the tensile and compressive reinforcement in the flange. To encounter reversal of loads, A'_s is set to be equal to A_s. The compressive force C_c consists of two parts

$$C_c = C_{c1} + C_{c2} \tag{3.14}$$

and

$$C_{c1} = 0.85 f'_c \times (b_f - t) \times t_f$$

$$C_{c2} = 0.85 f'_c \beta_1 c t$$

where

- c: distance from the extreme compressive fiber to the neutral axis
- β_1: 0.85 for $f'_c = 4000$ psi
- t: thickness of wall
- b_f: width of flange; b_f is taken as 18 in
- t_f: thickness of flange; t_f is taken as 12 in

Substituting Eqs. 3.12–3.14 into Eq. 3.11, c is determined as 21.0 in. Taking moments about the center of tensile reinforcement, the equilibrium of moment results in the following equation.

$$P_n(e + \frac{d - t_f/2}{2}) = C_{c1}(d - t_f/2) + C_{c2}(d - \frac{\beta_1 c}{2}) + C_s(d - t_f/2) \tag{3.15}$$

where d is the distance from the extreme compressive fiber to the centroid of tensile reinforcement. Solving Eq. 3.15, the required tensile reinforcement area A_s is 7.6 in^2. Thus, 8-#9 rebars ($A_s = 8.0$ in^2) are used.

2) Case 4: $P_u = 367.5$ kips, $M_u = 7752$ ft-kips

The required nominal axial strength P_n and the nominal flexure strength M_n are

$$P_n = \frac{P_u}{\phi} = 525 \text{ kips}$$

$$M_n = \frac{M_u}{\phi} = 11074.3 \text{ ft} - \text{kips}$$

Thus, the eccentricity is determined as 21.1 ft. It is assumed that the compressive reinforcement does not yield, while the tensile reinforcement has yielded. Thus,

$$T = A_s f_y$$

$$C_s = E_s \epsilon_s' A_s \tag{3.16}$$

Furthermore, it is assumed that the neutral axis is located within the flange.

$$C_c = 0.85 f_c' b_f \beta_1 c \tag{3.17}$$

Substituting Eqs. 3.16 and 3.17 into Eq. 3.11, A_s can be expressed as

$$A_s = \frac{525c - 52c^2}{27c - 525} \tag{3.18}$$

Taking moments about the center of tensile reinforcement and using Eq. 3.18, c is determined as 11.85 in. Substituting c into Eq. 3.18, A_s is determined as 5.3 in^2 which is less than 7.6 in^2 required by case 3. Thus, $8 - \#9 (A_s = 8.0 \text{ in}^2)$ provide enough resistance.

3) Cases 1 and 2

For cases 1 and 2, the shear wall is subjected to axial force only. As shown in Table 3-VI, the maximum factored axial force P_u for cases 1 and 2 is 790.0 kips. The ACI code specified that the required axial force strength P_n is

$$P_n = \frac{0.8}{\phi}[0.85 f_c'(A_g - A_{st}) + f_y A_{st}] \tag{3.19}$$

where

ϕ: strength reduction factor; $\phi = 0.7$

A_g: gross area of wall section

A_{st}: total area of longitudinal reinforcement

It can be easily shown that the shear wall designed for cases 3 and 4 has much larger axial strength than that required by cases 1 and 2. The detail of shear wall and the arrangement of reinforcement are shown in Fig. 3-2.

3.5 Ground Motion Characterization

The shear wall structure is evaluated at two PGA levels. The seismic hazard curves for rock sites in the Memphis area are shown in Ref. 23. From these curves, the PGA value of the maximum probable earthquake is determined as 0.18 g, while the PGA of the maximum credible earthquake is 0.32 g. However, Memphis is located in Mississippi Embayment and thus the PGA value obtained under rock condition needs to be modified to include soil effects. The soil amplification factor for Memphis may range from 1.4 to 2.2 [24]. Thus, the PGA of the maximum probable earthquake may become 0.32 g if the soil effects are included.

The earthquake ground motion used in this study is represented by an ensemble of artificial time histories generated from two Kanai-Tajimi power spectra. Two parameters of each Kanai-Tajimi power spectrum, namely ω_g and ζ_g in Eq. 2.29, need to be determined in order to simulate earthquakes. These two parameters depend on the site soil conditions. In this study, we do not focus on a structure at a specific site. Rather, our attention is to a class of structures which may be located at different sites within the region considered. Thus, general understanding of soil conditions in the region is sufficient for this study. Memphis is known as part of the Mississippi Embayment. The soil deposits in Memphis range from soft to stiff soil. Therefore, two power spectra are utilized in this study; one represents stiff soil, while the other represents soft soil. For stiff soil, ω_g and ζ_g are taken to be 5π rad/sec and 0.6, and for soft soil, ω_g and ζ_g are chosen to be 2.4π rad/sec and 0.85 [25]. The two power spectra in accordance with these two soil conditions are shown in Fig. 3-3. From each power spectrum, stationary time histories are generated first by using Eq. 2.28 in which different random phase angles are used. The envelope function used in Eq. 2.30 is assumed to be a trapezoidal shape with total duration of 15 sec as shown in Fig. 3-4. The nonstationary time histories are then obtained from the product of the envelope function and stationary time histories. A sample of nonstationary acceleration time history

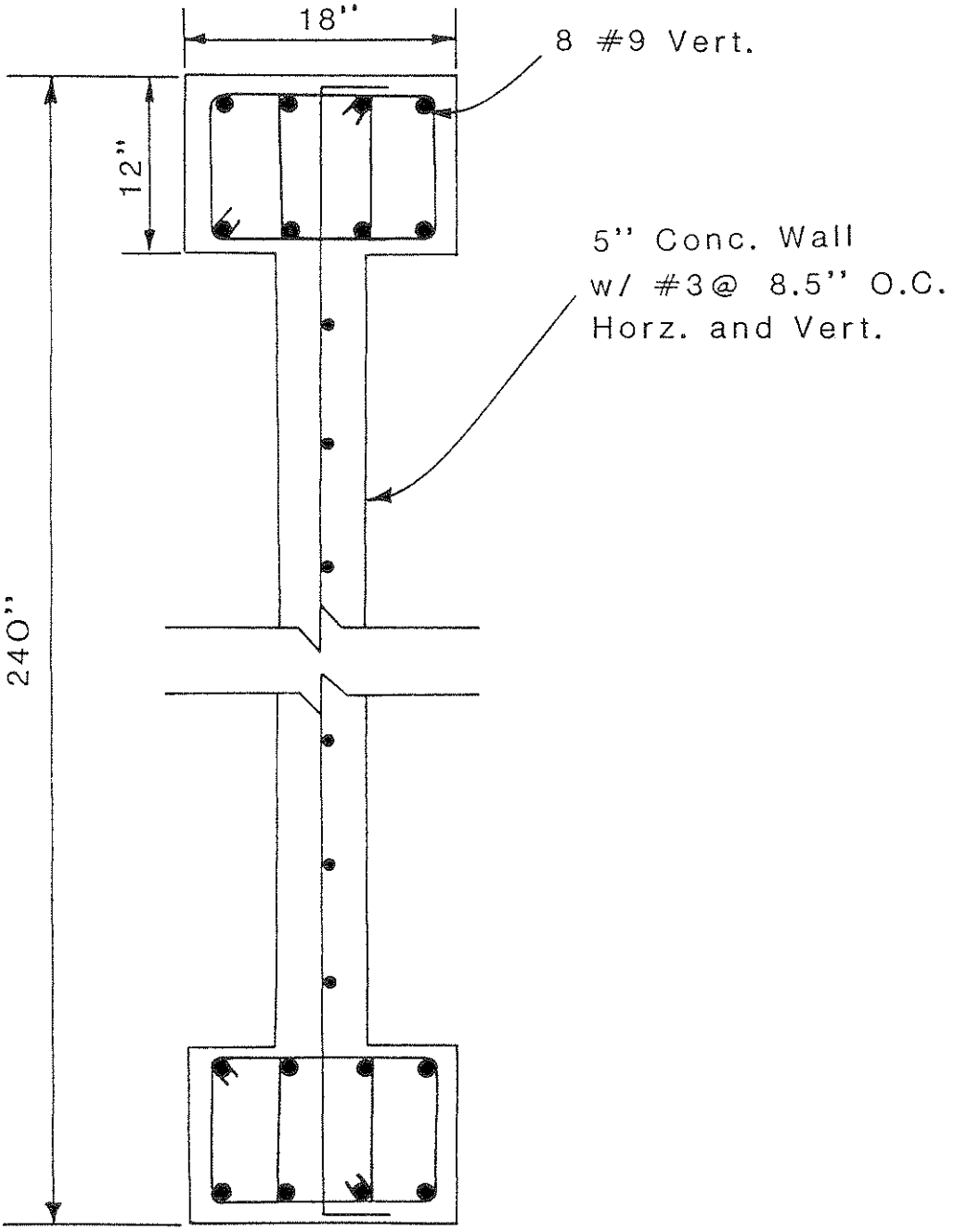

Fig. 3-2 Detail of Shear Wall

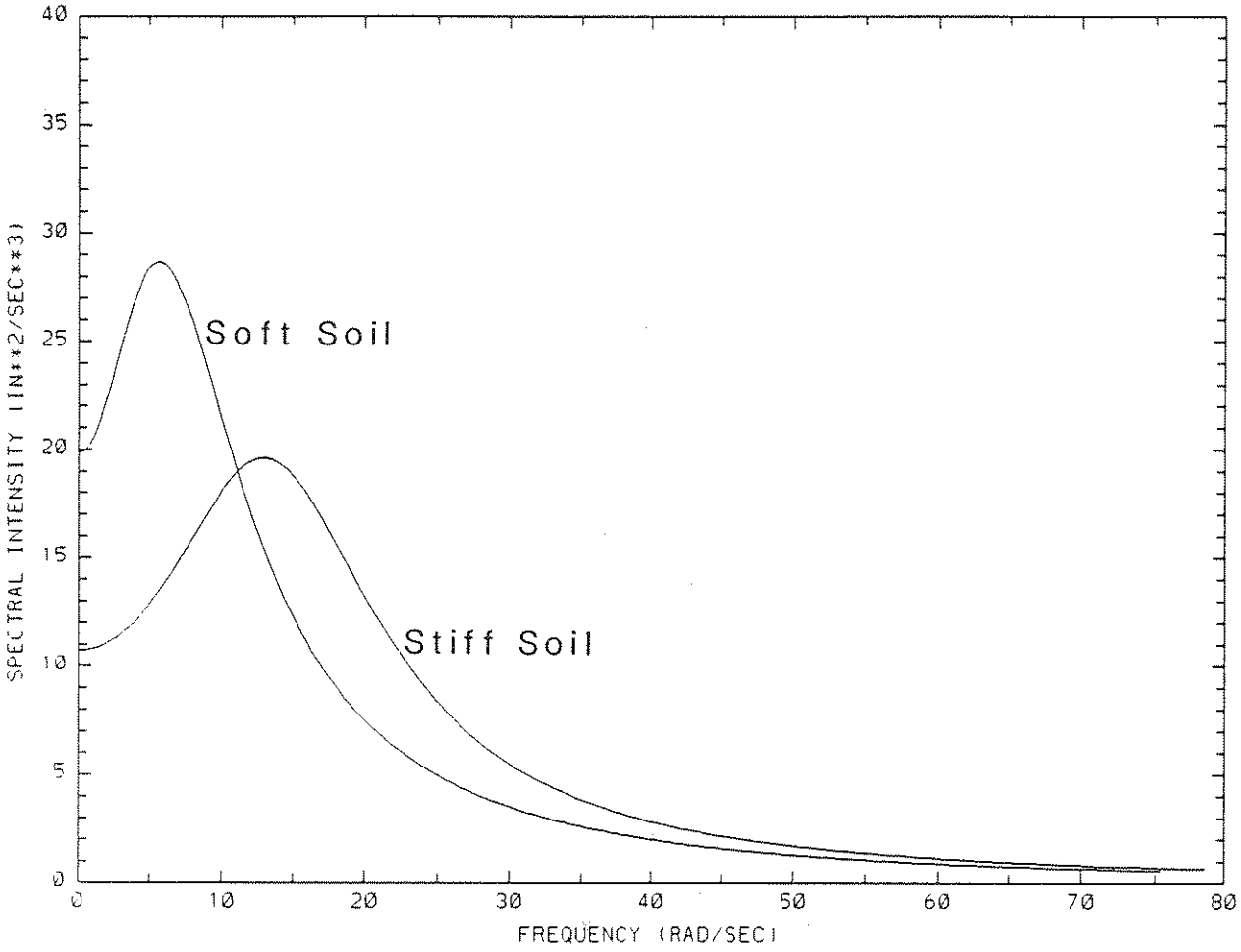

Fig. 3-3 Power Spectra

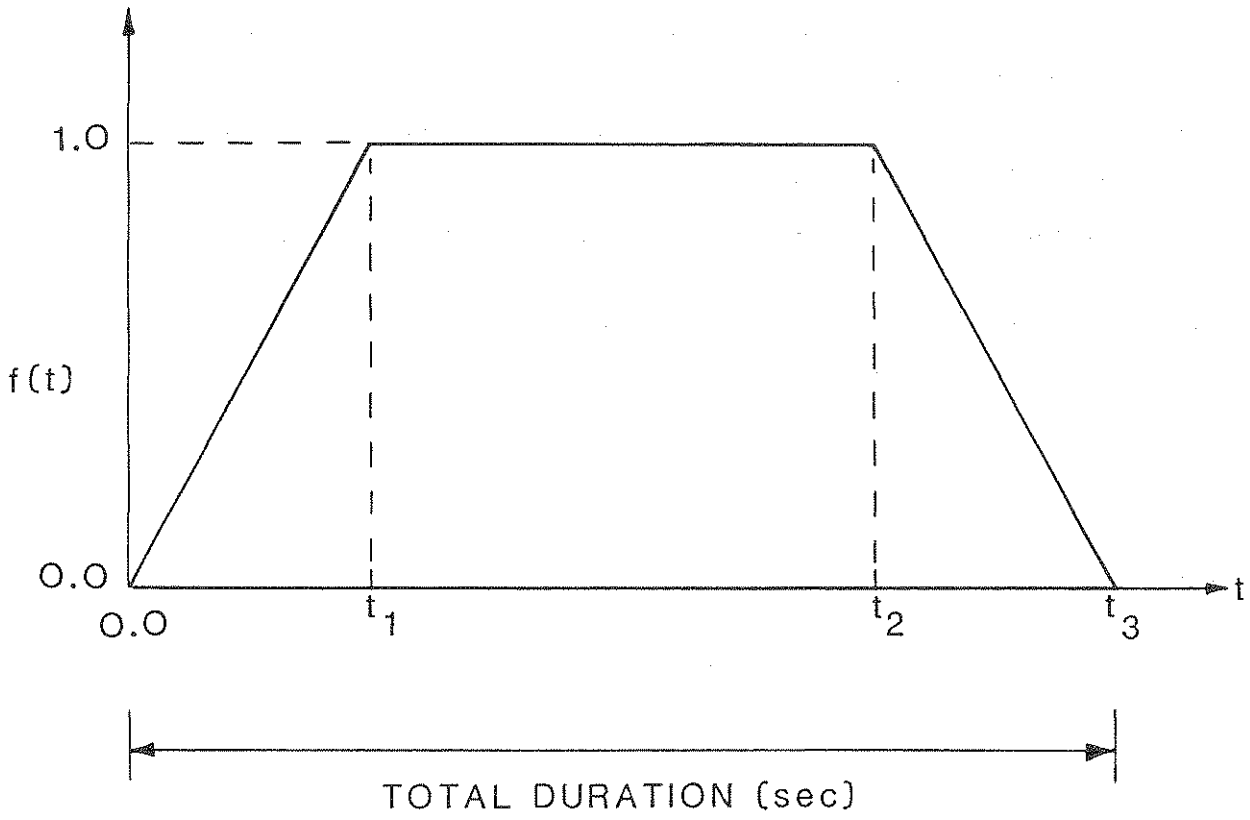

Fig. 3-4 Envelope Function

is shown in Fig. 3-5. For each PGA level, 25 artificial earthquakes are generated for each power spectrum. Thus, a total of 50 earthquakes are obtained for each PGA level.

3.6 Structural Modeling

The shear wall structure is idealized as a stick model with fixed base as shown in Fig. 2-2. The stick model consists of story masses concentrated at nodes connected by shear beam elements. The story mass M_1, M_2, and M_3 are 1.199, 1.165 and 0.878 kips-sec^2/in, respectively. The shear force-displacement relationship of each element follows the modified Takeda hysteretic rules. The parameters defining the hysteretic model are initial stiffness k_e, post-yielding stiffness k_p, yielding displacement U_y, and pinching factor α_p.

The initial stiffness k_e is less than so-called uncracked shear stiffness k_o due to the existence of shear cracks. For each element, the initial stiffness is determined as

$$k_e = \frac{GA_s}{h} \tag{3.20}$$

where

G: cracked shear modulus
A_s: effective shear area
h: height of beam element

For a shear wall with two boundary columns, the effective shear area is the area of the web. The height and effective shear area of the beam elements are shown in Table 3-VII. The cracked shear modulus G is expressed as

$$G = \alpha_g G_0 \tag{3.21}$$

in which G_0 is the uncracked shear modulus of the beam element.

$$G_0 = \frac{E_c}{2(1-\nu)} \tag{3.22}$$

where E_c is the Young's modulus of concrete. For $f'_c = 4000$ psi, E_c is equal to 3.6×10^6 psi. The Poisson's ratio ν is assumed to be 0.2 in this study. Thus, G_0 is 1.5×10^6 psi

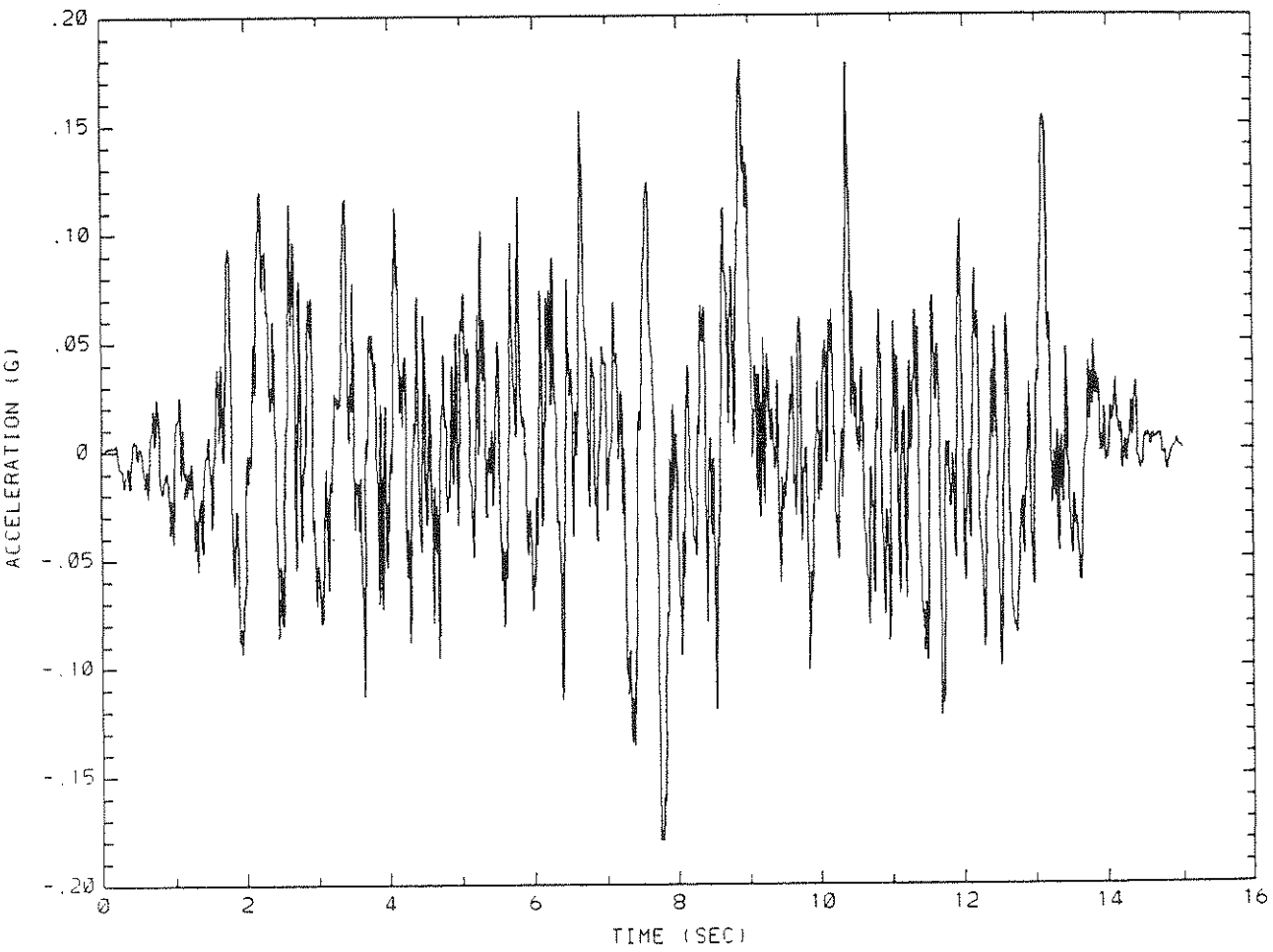

Fig. 3-5 A Sample of Artificial Earthquakes

Table 3-VII Height and Shear Area of Elements

Element No.	h (in)	$A_s(\text{in}^2)$
3	180	1080
2	180	1080
1	240	1080

(Eq. 3.22). In this study, α_g is taken as 0.15 and thus G is determined to be 2.25×10^5 psi. The post-yielding stiffness is expressed as a product of post-yielding slope factor α_s and initial stiffness k_e. The post-yielding slope factor of the beam element is 0.04 from load-deformation curves of shear walls under cyclic loads [26]. The yielding shear strain is taken as 0.002. Thus, the yielding displacement U_y of the element can be determined from multiplying yielding shear strain by element height h. Given U_y, the corresponding yielding shear strength Q_y is derived from Eq. 2.4. Furthermore, the pinching factor α_p needs to be determined in order to complete the hysteretic model. By comparison of simulation and experimental results, Tohma and Hwang [9] suggested that a pinching factor of 0.3 would be an appropriate value to account for pinching phenomenon. Thus, the pinching factor α_p is set to be 0.3 for all elements for this study. The parameter values of the hysteretic model are summarized in Table 3-VIII.

The damping of structure is assumed to be the Rayleigh damping as described by Eq. 2.2. From the modal analysis of the structural system, the natural frequencies of the first two modes are 14.80 rad/sec and 42.26 rad/sec, respectively. The critical damping ratio ζ for these two modes are assumed to be 4 percent. The coefficients of the damping matrix, a_0 and a_1 in Eq. 2.3 are determined as 0.88 and 0.0014, respectively.

3.7 Response Statistics

For each artificial earthquake, a nonlinear seismic analysis of the structure is performed. It is observed from the results of these nonlinear seismic analyses that the shear wall structure under severe earthquakes exhibits nonlinear behavior in element 1 (first story), while the second and third elements still remain elastic. Tables 3-IX and 3-X present the 50 maximum ductility ratios for PGA of 0.18 g and 0.32 g, respectively. For PGA of 0.18 g, the maximum ductility ratios range from 0.75 to 2.04 with the mean value equals 1.1 and coefficient of variation (COV) is 0.24. The maximum ductility ratio μ_E is assumed to follow the extreme Type I distribution. The parameters α and u which define the extreme Type I distribution can be determined from the statistics of maximum ductility ratios (Eq. 2.35). For PGA of 0.18 g, α and u are determined as 4.8442 and 0.98235, respectively. For PGA of 0.32 g, the maximum ductility ratios vary from 1.46 to 3.69. The mean value is determined as 2.27 and COV is 0.25. The extreme Type I distribution parameters α and u are determined to be 2.2691 and 2.0182, respectively.

Table 3-VIII Parameter Values of Hysteretic Model

Element No.	U_y (in)	k_e (kips/in)	k_p(kips/in)	α_p
3	0.36	1350	54	0.3
2	0.36	1350	54	0.3
1	0.48	1012.5	40.5	0.3

Table 3-IX Maximum Ductility Ratios for PGA = 0.18g

0.9604	0.9750	1.0583	1.4167	1.3958
1.4417	1.4125	0.8854	1.1667	2.0438
1.0688	0.8938	1.3000	1.0270	1.0792
0.8688	1.6208	0.9188	1.3333	0.7500
0.7604	1.0021	1.1833	0.8125	1.2521
0.8292	1.5333	1.1729	0.8354	0.9229
1.5020	0.9229	1.0417	0.9063	1.2333
0.7550	1.4625	1.1000	1.1042	1.0438
1.2375	1.0625	0.8063	0.9021	1.2125
0.9979	1.1688	0.7854	0.8646	1.0250

Table 3-X Maximum Ductility Ratios for PGA = 0.32g

2.1083	1.7563	2.4875	1.8000	2.0938
2.3146	2.1188	2.1688	2.2938	2.6479
2.7438	2.1292	3.3500	2.8875	1.7688
1.8792	2.4688	2.0917	2.2771	1.4979
1.4583	2.1229	1.9563	1.9813	2.2833
1.6250	2.4146	2.5979	1.5542	1.8708
1.5833	3.6854	2.2979	1.5000	2.9104
1.8771	3.3833	1.9229	2.2854	2.1958
3.2375	2.8292	1.5521	3.0125	2.8250
1.7042	2.2188	3.6604	2.0354	2.1625

3.8 Seismic Performance Assessment

In the event of earthquakes, damage of buildings is observed to vary from no damage to collapse. In the present study, two limit states representing the moderate structural damage and collapse of structure are established. The ductility capacity μ_R associated with a particular limit state is assumed to be lognormally distributed. For the limit state corresponding to collapse of structure, the median capacity $\tilde{\mu}_R$ and the logarithmic standard deviation β_R are determined as 7.5 and 0.3, respectively, using test data of shear wall specimens [27]. For the limit state representing moderate structural damage, the median capacity $\tilde{\mu}_R$ of 4 and β_R of 0.3 are assigned based on the engineering judgement. The conditional limit state probabilities for these two limit states are computed using Eq. 2.37 and tabulated in Table 3-XI.

On the basis of the limit state probabilities listed in Table 3-XI, the following observations are made. Given the occurrence of an earthquake with PGA of 0.18 g, the probability of collapse of shear wall structure is very small. Although the probability of moderate structural damage is about three orders larger than the probability of structural collapse, the chance for the structure to incur moderate damage due to a 0.18 g earthquake is still very slim. However, if an earthquake with PGA of 0.32 g occurs, it is expected that one out of one thousand low-rise shear wall structures will collapse and about six percent will sustain moderate damage. With these limit state probabilities available, the authority can evaluate the societal risk due to earthquakes and make decision on which level of earthquake protection is appropriate.

Table 3-XI Limit State Probabilities

PGA	Moderate Structural Damage	Collapse
0.18 g	4.0×10^{-4}	5.4×10^{-7}
0.32 g	6.2×10^{-2}	1.0×10^{-3}

SECTION 4
SUMMARY AND CONCLUSIONS

This report presents a method to assess the actual seismic performance of code-designed structures, in particular, shear wall structures. For illustration, a three-story shear wall building located in Memphis is designed according to the seismic provisions stipulated in ANSI A58.1-1982 and ACI 318-83. For assessing seismic performance of structures, a probabilistic approach is used so that uncertainties in earthquake ground motions, structural responses, and structural capacities can be taken into consideration. Uncertainty in earthquake ground accelerations is explicitly accounted for by generating an ensemble of acceleration time histories from appropriate power spectral density functions and duration of strong motion. Two power spectra are employed in this study to represent variation of earthquake frequency contents due to local soil conditions.

The hysteretic relationship between the restoring force and inter-node displacement is established to describe the nonlinear structural behavior. In this study, the modified Takeda hysteretic model is utilized and the model includes a bilinear skeleton curve, degradation of stiffness and pinching effect. The structural responses are obtained from time history analysis and Newmark's beta method is utilized to integrate the equations of motion. The maximum ductility ratios obtained from time history analyses are then analyzed statistically. In this study, two limit states in terms of the maximum ductility ratio are established. One limit state represents the collapse of structures while the other represents the moderate damage of structures. The probabilistic distribution of the structural capacities can be established based on the defined limit states.

The performance of structures is measured in terms of the limit state probability, i.e., the probability that the structural response due to earthquake exceeds the structural capacity. It is noted that the methodology may be applied to various different types of structures to evaluate the limit state probabilities which are used to assess the actual performance of structures under earthquakes. Given the limit state probabilities, e.g. those shown in Table 3-XI, the authority can consider the societal risk due to the occurrence of earthquakes and make decision on which level of earthquake protection is appropriate.

SECTION 5
REFERENCES

1. International Conference of Building Officials, *Uniform Building Code*, 1985 Edition, Whittier, California, 1985.

2. Southern Building Code Congress International, *Standard Building Code*, 1985 Edition, Birmingham, Alabama, 1985.

3. American National Standards Institute, *Minimum Design Loads for Buildings and Other Structures*, ANSI A58.1-1982, New York, 1982.

4. Building Officials and Code Administrators International, *The BOCA Basic Building Code*, 1981 Edition, Homewood, Illinois, 1981.

5. American Insurance Association, *The National Building Code*, 1976 Edition, New York, 1976.

6. Applied Technology Council, "Tentative provisions for the Development of Seismic Regulations for Buildings," ATC 3-06, National Bureau of Standards, Washington, D.C., 1978.

7. Building Seismic Safety Council, "NEHRP Recommended Provisions for the Development of Seismic Regulations for New Buildings," 1985 Edition, Washington, D.C., 1985.

8. Whitman, R.V., "The Prognosis for Earthquake Hazard Mitigation," Proceedings of 3rd U.S. National Conference on Earthquake Engineering, Charleston, South Carolina, Vol. IV, Earthquake Engineering Research Institute, 1986, pp. 2617-2629.

9. Tohma, J. and Hwang, H., "Hysteretic Model for Reinforced Concrete Containment," Transaction of the 9th International SMiRT Conference, Lausanne, Switzerland, August 17-21, 1987, Vol. H, pp. 251-256.

10. Jennings, P.C., Housner, G.W., and Tsai, N.C., "Simulated Earthquake Motions," Earthquake Engineering Research Laboratory, California Institute of Technology, April 1968.

11. Ruiz, P. and Penzien, J., "Stochastic Seismic Response of Structures," Journal of Engineering Mechanics, ASCE, Vol. 94, No. EM2, April 1971, pp 441-456.

12. Shinozuka, M. and Jan, C-M., "Digital Simulation.of Random Processes and its Applications," Journal of Sound and Vibration, Vol. 25, No. 1, 1972, pp. 111-128.

13. Gasparini, D.A. and Vanmarcke, E.H., "SIMQKE, A program for Artificial Motion Generation," Dept. of Civil Engineering, Massachusetts Institute of Technology, November 1976.

14. Shinozuka, M., Deodatis, G. and Harada, T., "Digital Simulation of Seismic Ground Motion," NCEER-87-0017, National Center for Earthquake Engineering Research, August 1987.

15. Tajimi, H., "A Statistical Method of Determining the maximum Response of a Building Structure During an Earthquake," Proceedings of the 2nd World Conference on Earthquake Engineering, Tokyo, Vol. II, July 1960, pp. 781-798.

16. Shinozuka, M., Hwang, H., and Reich, M., "Reliability Assessment of Reinforced Concrete Containment Structures," Nuclear Engineering and Design, Vol. 80, 1984, pp. 247-267.

17. Jaw, J.-W., and Hwang, H., "Seismic Fragility Analysis of Shear Wall Structures," NCEER Technical Report (in preparation).

18. Penzien, J. and Liu, S.C., "Nondeterministic Analysis of Nonlinear Structures Subjected to Earthquake Excitations," Proceedings of the 4th World Conference on Earthquake Engineering, Santiago, Chile, Vol. I, Section A-1, January, 1969, pp. 114-129.

19. Ang, A. H.-S. and Tang, W.H., *Probability Concepts in Engineering Planning and Design*, Vol. II, John Wiley and Sons, Inc., New York, 1984.

20. Chung, Y.S., Meyer, C., and Shinozuka, M., "Seismic Damage Assessment of Reinforced Concrete Members," Technical Report NCEER-87-0022, National Center for Earthquake Engineering Research, October 1987.

21. Ellingwood, B., and Hwang, H., "Probabilistic Descriptions of Resistance of Safety-related Structures in Nuclear Power Plants," Nuclear Engineering and Design, Vol. 88, 1985, pp. 169-178.

22. American Concrete Institute, *Building Code Requirements for Reinforced Concrete*, ACI 318-83, Detroit, Michigan.

23. Algermissen, S.T., et al., "Probabilistic Estimates of Maximum Acceleration and Velocity in Rock in the Contiguous United States," USGS Open-File Report 82-1033, 1982.

24. Hwang, H., Low, Y.K., Jaw, J.-W., and Chang, T.-S., "Soil Effects on Strong Earthquake Acceleration in Memphis Area," CERI Technical Report, Memphis State University, February 1988.

25. Ellingwood, B. and Batts, M., "Characterization of Earthquake Forces for Probability Based Design of Nuclear Structures," NUREG/CR-2945, U.S. Nuclear Regulatory Commission, Washington, D.C., September 1982.

26. Oesterle, R.G., et al., "Web Crushing of Reinforced Concrete Structural Walls," ACI Journal, May-June 1984, pp. 231-241.

27. Aktan, A.E. and Bertero, V.V., "RC Structural Walls: Seismic Design for Shears," Journal of Structural Engineering, ASCE, Vol. 111, No. 8, August 1985, pp. 1775-1791.

NATIONAL CENTER FOR EARTHQUAKE ENGINEERING RESEARCH
LIST OF PUBLISHED TECHNICAL REPORTS

The National Center for Earthquake Engineering Research (NCEER) publishes technical reports on a variety of subjects related to earthquake engineering written by authors funded through NCEER. These reports are available from both NCEER's Publications Department and the National Technical Information Service (NTIS). Requests for reports should be directed to the Publications Department, National Center for Earthquake Engineering Research, State University of New York at Buffalo, Red Jacket Quadrangle, Buffalo, New York 14261. Reports can also be requested through NTIS, 5285 Port Royal Road, Springfield, Virginia 22161. NTIS accession numbers are shown in parenthesis, if available.

NCEER-87-0001 "First-Year Program in Research, Education and Technology Transfer," 3/5/87, (PB88-134275/AS).

NCEER-87-0002 "Experimental Evaluation of Instantaneous Optimal Algorithms for Structural Control," by R.C. Lin, T.T. Soong and A.M. Reinhorn, 4/20/87, (PB88-134341/AS).

NCEER-87-0003 "Experimentation Using the Earthquake Simulation Facilities at University at Buffalo," by A.M. Reinhorn and R.L. Ketter, to be published.

NCEER-87-0004 "The System Characteristics and Performance of a Shaking Table," by J.S. Hwang, K.C. Chang and G.C. Lee, 6/1/87, (PB88-134259/AS).

NCEER-87-0005 "A Finite Element Formulation for Nonlinear Viscoplastic Material Using a Q Model," by O. Gyebi and G. Dasgupta.

NCEER-87-0006 "SMP - Algebraic Codes for Two and Three Dimensional Finite Element Formulations," by X. Lee and G. Dasgupta, to be published.

NCEER-87-0007 "Instantaneous Optimal Control Laws for Tall Buildings Under Seismic Excitations," by J.N. Yang, A. Akbarpour and P. Ghaemmaghami, 6/10/87, (PB88-134333/AS).

NCEER-87-0008 "IDARC: Inelastic Damage Analysis of Reinforced Concrete-Frame Shear-Wall Structures," by Y.J. Park, A.M. Reinhorn and S.K. Kunnath, 7/20/87, (PB88-134325/AS).

NCEER-87-0009 "Liquefaction Potential for New York State: A Preliminary Report on Sites in Manhattan and Buffalo," by M. Budhu, V. Vijayakumar, R.F. Giese and L. Baumgras, 8/31/87, (PB88-163704/AS).

NCEER-87-0010 "Vertical and Torsional Vibration of Foundations in Inhomogeneous Media," by A.S. Veletsos and K.W. Dotson, 6/1/87, (PB88-134291/AS).

NCEER-87-0011 "Seismic Probabilistic Risk Assessment and Seismic Margin Studies for Nuclear Power Plants," by Howard H.M. Hwang, 6/15/87, (PB88-134267/AS).

NCEER-87-0012 "Parametric Studies of Frequency Response of Secondary Systems Under Ground-Acceleration Excitations," by Y. Yong and Y.K. Lin, 6/10/87, (PB88-134309/AS).

NCEER-87-0013 "Frequency Response of Secondary Systems Under Seismic Excitations," by J.A. HoLung, J. Cai and Y.K. Lin, 7/31/87, (PB88-134317/AS).

NCEER-87-0014 "Modelling Earthquake Ground Motions in Seismically Active Regions Using Parametric Time Series Methods," G.W. Ellis and A.S. Cakmak, 8/25/87, (PB88-134283/AS).

NCEER-87-0015 "Detection and Assessment of Seismic Structural Damage," by E. DiPasquale and A.S. Cakmak, 8/25/87, (PB88-163712/AS).

NCEER-87-0016 "Pipeline Experiment at Parkfield, California," by J. Isenberg and E. Richardson, 9/15/87, (PB88-163720/AS).

NCEER-87-0017 "Digital Simulations of Seismic Ground Motion," by M. Shinozuka, G. Deodatis and T. Harada, 8/31/87, (PB88-155197/AS).

NCEER-87-0018 "Practical Considerations for Structural Control: System Uncertainty, System Time Delay and Truncation of Small Forces," J. Yang and A. Akbarpour, 8/10/87, (PB88-163738/AS).

NCEER-87-0019 "Modal Analysis of Nonclassically Damped Structural Systems Using Canonical Transformation," by J.N. Yang, S. Sarkani and F.X. Long, 9/27/87.

NCEER-87-0020 "A Nonstationary Solution in Random Vibration Theory," by J.R. Red-Horse and P.D. Spanos, 11/3/87, (PB88-163746/AS).

NCEER-87-0021 "Horizontal Impedances for Radially Inhomogeneous Viscoelastic Soil Layers," by A.S. Veletsos and K.W. Dotson, 10/15/87, (PB88-150859/AS).

NCEER-87-0022 "Seismic Damage Assessment of Reinforced Concrete Members," by Y.S. Chung, C. Meyer and M. Shinozuka, 10/9/87, (PB88-150867/AS).

NCEER-87-0023 "Active Structural Control in Civil Engineering," by T.T. Soong, 11/11/87.

NCEER-87-0024 "Vertical and Torsional Impedances for Radially Inhomogeneous Viscoelastic Soil Layers," by K.W. Dotson and A.S. Veletsos, 12/87.

NCEER-87-0025 "Proceedings from the Symposium on Seismic Hazards, Ground Motions, Soil-Liquefaction and Engineering Practice in Eastern North America, October 20-22, 1987, edited by K.H. Jacob, 12/87.

NCEER-87-0026 "Report on the Whittier-Narrows, California, Earthquake of October 1, 1987," by J. Pantelic and A. Reinhorn, 11/87.

NCEER-87-0027 "Design of a Modular Program for Transient Nonlinear Analysis of Large 3-D Building Structures," by S. Srivastav and J.F. Abel, 12/30/87.

NCEER-88-0001 "Workshop on Seismic Computer Analysis and Design With Interactive Graphics," by J.F. Abel and C.H. Conley, 1/18/88.

NCEER-88-0002 "Optimal Control of Nonlinear Structures," J.N. Yang, F.X. Long and D. Wong, 1/22/88.

NCEER-88-0003 "Substructuring Techniques in the Time Domain for Primary-Secondary Structural Systems," by G. D. Manolis and G. Juhn, 2/10/88, to be published.

NCEER-88-0004 "Iterative Seismic Analysis of Primary-Secondary Systems," by A. Singhai, L.D. Lutes and P. Spanos, 2/23/88.

NCEER-88-0005 "Stochastic Finite Element Expansion for Random Media," P. D. Spanos and R. Ghanem, 3/14/88, to be published.

NCEER-88-0006 "Combining Structural Optimization and Structural Control," F. Y. Cheng and C. P. Pantelides, 1/10/88, to be published.

NCEER-88-0007 "Seismic Performance Assessment of Code-Designed Structures," Howard H.M. Hwang, J. Jaw and H. Shau, 3/20/88, to be published.